Applications in Energy and Combustion Science 14 (2023) 100132

Contents lists available at ScienceDirect

Applications in Energy and Combustion Science

journal homepage: www.sciencedirect.com/journal/applications-in-energy-and-combustion-science

Generalizing progress variable definition in CFD simulation of combustion systems using tabulated chemistry models

Pourya Rahnama [a,b,*], Amin Maghbouli [c], Hesheng Bao [a], Aromal Vasavan [a], Ricardo Novella [b], Bart Somers [a]

[a] Power & Flow – Department of Mechanical Engineering, The Technical University of Eindhoven, P.O. Box 513, Eindhoven, MB 5600, the Netherlands
[b] CMT – Motores Térmicos, Universidad Politécnica de Valencia, Camino de Vera s/n, Valencia E-46022, Spain
[c] Alumni, Department of Energy, Politecnico di Milano, Campus Bovisa - Via Lambruschini, 4a, Milano 20156, Italy

ARTICLE INFO

Keywords:
Flamelet models
Tabulated chemistry models
Computational fluid dynamics
Spray A
Progress variable
Non-premixed flame

ABSTRACT

In the Computational Fluid Dynamics (CFD) simulation of advanced combustion systems, the chemical kinetics must be examined in detail to predict the emissions and performance characteristics accurately. Nevertheless, the combustion simulation with detailed chemical kinetics is complicated because of the number of equations and a broad timescale spectrum. The Flamelet-Generated Manifold (FGM) is one of the examples of tabulation methods that has received much attention in recent years due to its fast and accurate prediction of combustion characteristics. The Progress Variable (PV) definition in FGM and other PV-based tabulated approaches is often selected randomly or depending on the user's experience. When complicated combustion systems are involved, such choices can become extremely difficult. In the current work, a generic approach for formulating a global PV is developed and tested in various operating conditions relevant to combustion engines. The method is based on a genetic algorithm optimization to maximize the monotonicity of PV, ensuring that for each value of PV, the dependent thermophysical properties have unique values. The FGM model's ability to reproduce the detailed kinetics evolution of the essential combustion and emission parameters of a non-premixed diffusion flame in Spray A configuration is evaluated in both one-dimensional counterflow and CFD simulation. It is concluded that with the use of the current approach, important combustion characteristics can be predicted much better compared to non-optimized PV while eliminating the manual selection of PV definition by the user. Since the algorithm needs to be executed before the chemistry tabulation in the pre-processing step, it does not increase the runtime of the FGM simulation. The algorithm only needs a few minutes to be finished on a standard desktop. The improvement in the results and the distribution of the values of important species in the computational domain is examined.

1. Introduction

In recent years, the computational fluid dynamics (CFD) method to simulate flow fields and design advanced and complex systems has become very widespread in industry and academia. However, due to their high computational resources demand, the use of detailed kinetic models to simulate combustion in different practical problems is still restricted to simple chemical kinetic mechanisms and geometries [1]. In particular, the combustion simulation involves a wide range of time scales, and for each species, a partial differential equation (PDE) must be computed in the detailed kinetic approach [2,3]. Having a wide range of time scales escalates the stiffness of the differential equations, which forces very small time steps and/or the use of an advanced numerical technique to solve the system of equations [4]. In addition, each chemical mechanism for the combustion simulation of hydrocarbon fuel usually includes more than 100 species [5,6]. Nonetheless, the modeling of flames with detailed mechanisms has been done by several authors. Schluckner et al. [7] applied a detailed kinetic model to investigate NOx formation in an oxy-fuel combustion of natural gas inside an industrial jet burner. Luecke et al. [8] validated a chemical kinetic mechanism by predicting the ignition delay time of n-heptane and isooctane in a high-pressure environment. However, the use of detailed kinetic models

* Corresponding author at: Power & Flow – Department of Mechanical Engineering, The Technical University of Eindhoven, P.O. Box 513, Eindhoven, MB 5600, the Netherlands.
E-mail address: pouryarahnama@gmail.com (P. Rahnama).

https://doi.org/10.1016/j.jaecs.2023.100132
Received 24 November 2022; Received in revised form 23 March 2023; Accepted 23 March 2023
Available online 25 March 2023

is still limited to simple geometries, and the simulation lasts a very long time, making it difficult to do a parametric study with the developed model. On the other hand, simple methods such as one-step reaction models cannot predict the combustion and emission characteristics, such as the combustion characteristics in Dual Fuel combustion systems (see for example [9,10]), advanced engine combustion concepts like Homogeneous Charge Compression Ignition (HCCI) [11], Partial Premixed Compression Ignition (PPCI) [12], Reactivity Controlled Compression Ignition (RCCI) engines [13] or emission formation in post-injection strategies (for instance [14]). Combustion in these types of engines is kinetically controlled [15] and largely depends on the reactivity of the fuels as it controls the autoignition [16] as reviewed in [17]. Therefore, more advanced models are of great interest. These models are based on the high Damköhler number (Da) assumption. Da relates the flow time scale to the chemical reaction time scale. This assumption decouples the chemistry calculations from the flow field calculations, and it is the key hypothesis on which tabulated chemistry methods rely. The intrinsic low-dimensional manifold (ILDM) approach introduced by Maas and Pope [18] is one of the most famous models based on tabulating detailed chemistry. However, since it neglects the convection and diffusion terms in the transport equations, they are less applicable in low-temperature conditions where the chemical process is relatively slow, and the convection and diffusion become important and disturb the balance between chemical production and consumption [19].

The Flamelet Generated Manifold (FGM) [20] is a flamelet-based method like the Representative Interactive Flamelets (RIF) [21] and the multiple Representative Interactive Flamelet (mRIF) [22] that describes the turbulent flame as an ensemble of representative one-dimensional flames known as flamelets [23]. However, as opposed to the other flamelet methods, in FGM, the flamelets are pre-computed and stored. For this purpose, representative laminar 1-D flames (including convection and diffusion terms in the species transport equation) are simulated and pre-processed and then tabulated for a reduced number of controlling variables mapping the data on a low dimensional manifold [24]. This is achieved by a coordinate transformation from the space-time ($x-t$) domain to the control variables domain. Then the tabulated data is coupled back directly or with training Machine Learning techniques [25,69] with the flow field by transporting the complete set or a given selection of these control variables in the flow field [26]. The Flamelet Prolongation of ILDM (FPI) [27] and the Flamelet/Progress Variable (FPV) [28] are similar to the FGM. For instance, the FPV formulation is based on the steady flamelet model of Peters [29] and uses a single progress variable to describe the chemical kinetics and non-equilibrium chemistry. However, in the FGM multiple reaction control variables can be used. In these pre-computed flamelet models, the computational cost for the chemistry modeling is reduced as it is pre-processed while retaining the convection and diffusion effects. Pre-processing the stiff reaction equations decoupled from the turbulent flow field allows the use of relatively sizeable chemical reaction mechanism [30]. Nevertheless, the definition of the control variables should be such that the most relevant physical and chemical processes can be captured. In non-premixed combustion systems, these processes are mixing and chemical reactions. These two can be represented by a mixture fraction and a progress variable [31,32]. The effect of the fuel vaporization and the liquid phase can be included in the definition of the mixture fraction variable as shown in [33] or the fuel temperature can be reduced (as suggested in [34] and used by [35]). Mostly one PV is used as will be the case in this research though this is not a formal restriction. The PV definition is highly dependent on the type of fuel and the combustion system being simulated. For some hydrocarbons such as methane, a linear combination of CO_2, H_2O, and H_2 has proven to produce satisfactory results for non-premixed laminar flames [36]. For larger hydrocarbons, the combustion process is more complex and a different definition is required to capture the multiple stages of the combustion. In addition, when the operating condition or the configuration of the flame (like premixed or partially premixed) is changed, or when a second component is added to the fuel, the progress variable which results in appropriate precision for the pure fuel non-premixed flame cannot necessarily perform well in the new condition or configuration [37]. Therefore a general procedure is needed to select the progress variable definition automatically in different configurations and conditions, and assuring an accurate precision of predicting the most important combustion and emission characteristics, independent of the fuel used. This new technique for defining the progress variable will be beneficial in novel combustion applications where less knowledge is available, such as a dual fuel low-temperature combustion, a combustion with multiple reactant streams, and new fuel compositions.

The PV's main constraint is that it must increase or decrease monotonically, from the unburnt to the burnt side which means that each point in the thermochemical state space has to be represented by only one value for the progress variable [38]. In other words, for each value of the progress variable, there should be only one corresponding value for the thermophysical variables. In the literature, many empirical definitions of the progress variable have been used [39–41]. However, in some situations, these definitions may display a non-monotonic behavior that compromises the accuracy and even the applicability of the tabulated chemistry methods.

Ihme et al. [38], were among the first people who investigated the possibility of using an optimization technique to maximize the monotonicity of the progress variable. They found optimum progress variables for methane, methane/hydrogen, and an n-heptane/hydrogen one-dimensional diffusion and partially premixed flames using an unconstrained derivative-free pattern search algorithm. They found that the PV definition is dependent on each flame configuration and the fuel type. They also found that when all the species are included in the progress variable definition in the algorithm, the results can get better in terms of the cost function value. However, they did not assess the feasibility of the approach in a CFD problem. In the study of Niu et al. [42], a different objective function was used, so they minimized the gradients of the chemical species against the progress variable using the Simplex Algorithm and added the monotonicity as a constraint in the optimization problem. Nevertheless, depending on the fuel no solution might be found in this approach and this approach is based on an unsystematic choice of a threshold for minimizing the gradients. Hadadpour et al. [43] then used the same method to do a Large Eddy Simulation (LES) of spray combustion in a constant volume combustion chamber under operating conditions similar to combustion engines. But, they did not conduct a detailed investigation for the effect of this optimization and compare its performance with other common definitions in predicting important combustion parameters in different operating conditions. Prufert et al. [44], used a genetic algorithm and adopted the same objective function, but they added the non-monotonicity as a penalty factor in the objective function. They applied their method to a methane-air zero-dimensional homogeneous reactor, a laminar one-dimensional diffusion flame, and an oxyfuel flame. However, no implementation was performed in a CFD problem. Vasavan et al. [45] optimized the progress variable definition by a multi-objective genetic algorithm. They maximized the monotonicity and minimized the gradients in species concentrations against the progress variable. The results show that the FGM model with an optimum progress variable can reproduce the detailed results in three different configurations. Nonetheless, the FGM model was not implemented in a CFD solver to assess the capability of the method, and its applicability in reproducing the emissions profile was not studied. For instance, one of the major challenges faced during the CFD simulation of non-premixed diffusion flame is to predict the flame lift-off length (FLOL) and capture the two-stage ignition and the influence of PV optimization on the FLOL, the ignition characteristics, and the species mass fraction distribution in the domain needs to be investigated. More recently, Chitgarha et al. [46] used the FGM technique for CFD simulation of an ethanol-air flame in a

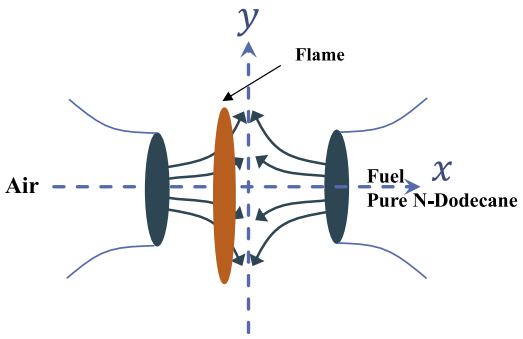

Fig. 1. Schematic diagram of counterflow diffusion flame (CDF).

different configuration (partially premixed two-dimensional counterflow). They adopted a genetic algorithm to optimize the progress variable definition with a different objective function compared to the other studies. They included the Damkohler number definition in the objective function to consider the effect of flow mixing time scale.

In this research, a generic approach for formulating a global progress variable (PV) with the Genetic Algorithm (GA) optimization technique will be developed and tested in a wide variety of operating conditions relevant to internal combustion engines for a non-premixed diffusion flame. Since in the non-premixed CFD simulation of diffusion flames, in addition to combustion, there are other important phenomena such as turbulent flow, spray, and evaporation, in this article, the governing equations for both FGM and detailed kinetics approaches are first used in one-dimensional counterflow problem. In the one-dimensional configuration, the errors related to the numerical solution in the CFD method, such as model verification errors of spray, turbulence, grid resolution, etc., are absent. Studying this configuration, where combustion and mixing are the only concerned phenomena, allows us to better recognize the performance of the FGM model with optimum progress variable (PV) over conventional and manually optimized PVs. Also, since in internal combustion engines, operating conditions such as pressure, oxidizer temperature, and strain rate are constantly changing, in the next stage, the performance of FGM on different working conditions in predicting the important parameters of combustion and emissions will be examined. The improvement of the monotonicity of PV for all values of mixture fraction is examined. Emission formation, ignition delay, and PV source term value are investigated in different pressure, temperature, and strain rates. After that, by implementing the FGM model in a CFD solver, the effect of optimization with the presence of phenomena such as turbulent flow, spray, and fuel evaporation is investigated. The improvement in the prediction of the important combustion parameters such as the ignition delay and the flame lift-off length (FLOL) of the spray A benchmark [47], as well as the distribution of the values of the key species in the computational domain, is studied.

2. Numerical methodology

2.1. FGM modeling approach

The FGM model for the counterflow diffusion flame is based on the flamelet equations obtained from the general conservation equations of mass, momentum, energy, and species including unsteady terms converted to a curvilinear coordinate system with the coordinate x perpendicular to the flame [48]. The influence of the y component of the flow (the tangential component of the flame surface) is considered by the local flame stretch rate parameter (K), which is equal to $K = \frac{\partial u_y}{\partial y}$. By introducing this parameter in the conservation equations, a new transport equation is obtained for the local flame stretch, and the following equations are formed.

$$\frac{\partial \rho}{\partial t} + \frac{\partial (\rho u)}{\partial x} = -\rho K \tag{1}$$

$$\frac{\partial \rho h}{\partial t} + \frac{\partial \rho u h}{\partial x} = \frac{\partial}{\partial x}\left(\frac{\lambda}{C_p}\frac{\partial h}{\partial x}\right) - \rho K h \tag{2}$$

$$\frac{\partial \rho Y_i}{\partial t} + \frac{\partial \rho u Y_i}{\partial x} = \frac{\partial}{\partial x}\left(\rho D \frac{\partial Y_i}{\partial x}\right) + \dot{\omega}_i - \rho K Y_i \tag{3}$$

$$\frac{\partial \rho K}{\partial t} + \rho u \frac{\partial K}{\partial x} = \frac{\partial}{\partial x}\left(\mu \frac{\partial K}{\partial x}\right) - \rho_{ox} a^2 - \rho K^2 \tag{4}$$

Where ρ and u are density and velocity, t is time, h is enthalpy, λ is conductivity, C_p is specific heat ratio, Y_i is species mass fraction, D is diffusion coefficient, $\dot{\omega}_i$ is the net change rate of species, μ is dynamic viscosity, and a is applied strain rate. Preferential diffusion effects are ignored by the assumption of unity Lewis number.

In deriving these equations, it is assumed that the flow in the far field behaves like a potential flow and a prescribed value for the gradient of the velocity or the strain rate on the oxidizer side of the counterflow configuration is considered (semi-infinite domain formulation). Therefore, the tangential pressure gradient term in the y-direction will be dependent on the applied strain rate at the boundary. It is also assumed that the flow and combustion variables are only a function of x and time, and only the pressure and the y component of the gas velocity are a function of both spatial coordinates. This formulation is different from Kee et al. [49] (which was also extended by Stahl and Warnatz [50] to unsteady problems) formulations where they obtain more accurate calculations for the tangential pressure gradient term (finite distance domain formulation). However, the formulation which is used here, is more convenient for the numerical implementation particularly when the detailed chemistry is considered.

The schematic of the Counterflow Diffusion Flame (CDF), as the representative flamelet in non-premixed combustion in the FGM model, is shown in Fig. 1. On the oxidizer side, the air is usually defined, and on the other side, a pure fuel like n-dodecane.

After the flamelet generation, the stored data is mapped to a new set of control variables (the manifold construction). The mapped data are used to calculate the same problem with less runtime and mathematical complexity in the FGM approach. In the FGM approach, only two transport equations are solved for mixture fraction and progress variable instead of solving the transport equations for all species. The two transport equations for CDF in the FGM approach can be written as follows:

$$\frac{\partial \rho PV}{\partial t} + \frac{\partial \rho u PV}{\partial x} = \frac{\partial}{\partial x}\left(\rho D \frac{\partial PV}{\partial x}\right) + \dot{\omega}_{PV} - \rho K PV \tag{5}$$

$$\frac{\partial \rho Z}{\partial t} + \frac{\partial \rho u Z}{\partial x} = \frac{\partial}{\partial x}\left(\rho D \frac{\partial Z}{\partial x}\right) - \rho K Z \tag{6}$$

Which together with Eqs. (1), and (4) complete the description of the CDF in the FGM approach. The PV is the progress variable, $\dot{\omega}_{PV}$ is the source term of the progress variable retrieved from the store table, and Z is the mixture fraction.

CHEM1D is used to calculate the governing equations of the 1D counterflow flame. CHEM1D [51] is software (implemented in Fortran programming language) for analyzing 1D reactive systems with both the detailed and FGM approach. Therefore, it is ideal for doing a preliminary study on the capability of FGM in capturing the non-premixed combustion behavior in the 1D setup. This code uses an exponential finite-volume discretization in space, and the resulting system is solved using a fully implicit, modified Newton technique. Adaptive gridding is also used to increase the resolution around the flame front. The default CHEM1D code does not provide the emission profile results of the FGM model, since in the FGM formulations, it is not needed to retrieve their

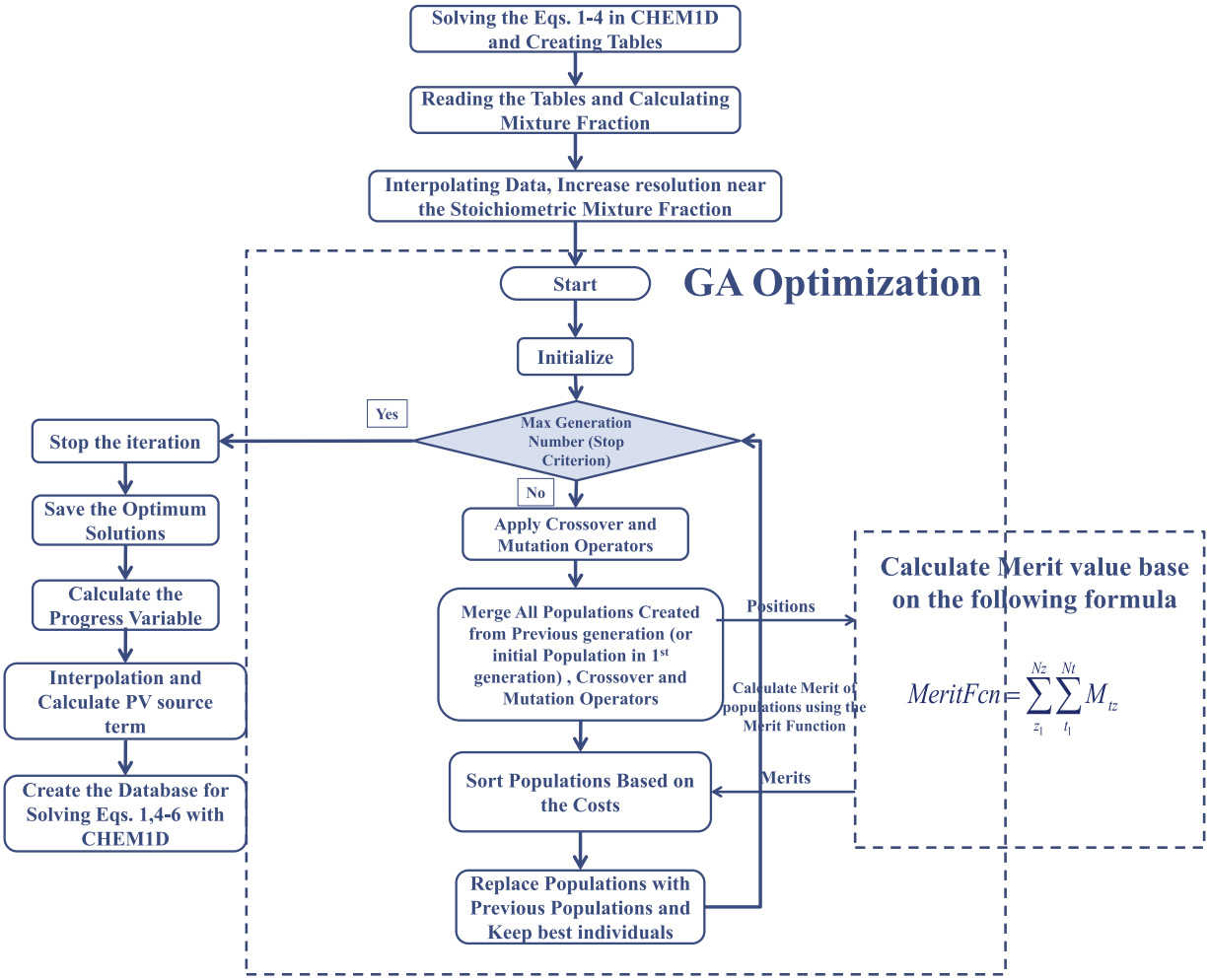

Fig. 2. Flowchart of the genetic algorithm optimization.

data from the tables. To compare the two models, the source code was modified to include the emission results. After obtaining the results from flamelet equations, they are mapped to the new coordinate system of the controlling variables using the MATLAB platform. The mapped data is then used in FGM simulation.

2.2. Genetic algorithm optimization

A genetic algorithm optimization technique will be adopted to develop a generic approach for the progress variable definition. As we discussed, the FGM results are highly dependent on the PV definition, and the selection of its definition requires a vast knowledge of combustion kinetics. Hence this generalized approach helps to automate the process of selecting PV definition in different combustion applications such as premixed, non-premixed, and partially premixed combustion systems. The GA is an evolutionary algorithm like the Strength Pareto Evolutionary Algorithm (SPEA). The advantage of these methods is that the final solution cannot easily become entrapped in the local optimum solution due to the random and stochastic nature of their operators. Therefore they are very appropriate in non-linear combustion systems (as it was used in [52]) in which the solution is prone to be entrapped in the local optimum. The GA starts with generating a random population. The population size should be higher when the number of optimization parameters increases. The merit or fitness of all individuals will be assessed, and parents are chosen according to their merits to create regular or mutated offspring [53]. The newly generated offspring are called the new generation and the process is repeated to find the best population [54]. It should be noted that each individual's fitness is defined based on the merit function that is evaluated for it. The method is generalizable and works based on the merit function defined and will find a solution that has the highest merit value. For this reason, the merit function defined in the algorithm can be changed to include other criteria in addition to the monotonicity of the progress variable. However, in combustion systems, the most important criterion for the progress variable is its monotonicity since it should show the combustion progress from the fuel decomposition to the final product formation. The whole procedure has been shown in [55]. Also, the GA algorithm here was implemented in MATLAB and the default MATLAB toolbox was not used to leave room for possible future research on the algorithm improvement in terms of finding the best possible optimum solution.

In the current study, the maximum number of generations was chosen as the number when the merit value of the best individual reached a steady state condition, and did not improve further. The population size should be chosen in such a way that it should be high enough to result in the highest possible merit value and it should be low enough not to cause a very long runtime. In this work, the population size was chosen with a low value and then it was gradually increased until its further increase did not improve the merit value. The other GA parameters such as mutation or crossover probability and selection pressure are tuned to achieve higher final merit values. Higher population numbers and greater mutation rates enhance diversity, but the population number should be selected with caution since it increases the algorithm runtime. The tuned parameters have been summarized in Appendix A.

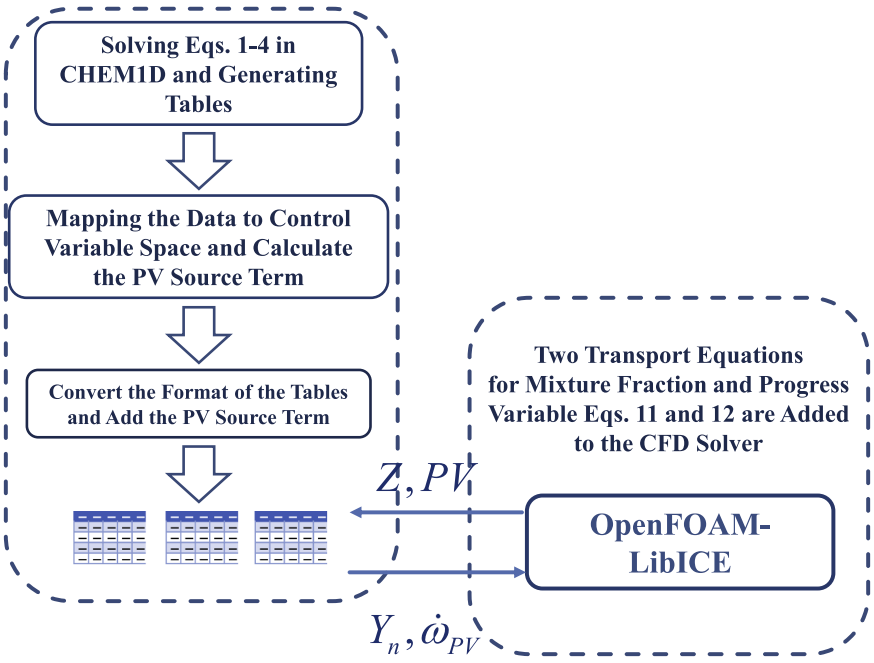

Fig. 3. The Implementation Method for the FGM Combustion Model for Simulating Turbulent Reacting Flows in a sector mesh.

The algorithm tries to find the best coefficients in the global formula for the progress variable which is defined as:

$$PV = \sum_{i=1}^{Nsp} a_i Y_i \tag{7}$$

Fig. 2 shows the flowchart of the optimization algorithm. The current study aims to maximize the monotonicity of the progress variable with respect to time and a merit function is defined accordingly. This ensures having unique values of the thermophysical properties for each value of the progress variable. Since the mixture fraction is the other independent variable in the FGM model, the progress variable must be monotonically increasing for all values of the mixture fraction. Therefore, the following formula is used to calculate the monotonicity, where N_z is the total number of the grid points in mixture fraction space, N_t is the total number of timesteps, t_1 and Z_1 denotes the values in the first timestep and mixture fraction grid, $PV_{\max}$ and $PV_{\min}$ are the maximum and minimum of progress variable in each grid point in mixture fraction space. M_{tz} is a mask matrix which gives zero to non-monotonic values, and unity to monotonic values. In other words, each individual's fitness is measured based on the number of unities in the mask matrix, and the algorithm finds the individual with the highest number in the mask matrix.

$$Monotonicity = \sum_{Z_1}^{N_z} \sum_{t_1}^{N_t} \frac{PV^{t_{i+1}} - PV^{t_i}}{PV_{\max} - PV_{\min}} \tag{8}$$

$$M_{tz} = \begin{cases} 1 & if \quad Monotonicity \geq 0 \\ 0 & if \quad Monotonicity < 0 \end{cases} \tag{9}$$

$$MeritFcn = \sum_{z_1}^{Nz} \sum_{t_1}^{Nt} M_{tz} \tag{10}$$

2.3. Turbulent flow modeling and combustion closure

After optimizing the progress variable in the 1D setup, the optimum progress variable is used to map the flamelet data from the x-t domain to the new Z-PV coordinate system (manifold generation). The mapped data is organized and sorted to be in the format readable by a CFD solver.

The final step is coupling the generated manifold with the flow field in the CFD solver. The coupling is performed by retrieving the data stored in the look-up tables via the controlling variables transported in the flow field. The CFD solver, in addition to the momentum and continuity equations, solves two extra transport equations for the mean (Favre-averaged) progress variable and the mixture fraction:

$$\frac{\partial \rho \bar{Z}}{\partial t} + \nabla.(\rho u \bar{Z}) - \nabla.\left(\left(\frac{\mu_t}{Sc_t} + \frac{\mu}{Sc}\right)\nabla \bar{Z}\right) = \bar{\dot{\omega}}_Z \tag{11}$$

$$\frac{\partial \rho \bar{PV}}{\partial t} + \nabla.(\rho u \bar{PV}) - \nabla.\left(\left(\left(\frac{\mu_t}{Sc_t} + \frac{\mu}{Sc}\right)\right)\nabla \bar{PV}\right) = \bar{\dot{\omega}}_{PV} \tag{12}$$

Sc is Schmidt number, where subscript t indicated turbulent values, $\bar{\dot{\omega}}_Z$ is the mean source term of mixture fraction owing to the spray evaporation, and $\bar{\dot{\omega}}_{PV}$ is the mean source term of the progress variable which is stored in the FGM tables.

In each time step, the governing equations in the CFD solver are used to calculate the mixture fraction and the progress variable for each computational cell. Subsequently, the calculated parameters will be sent to the tabulated data, and the values for the mass fraction of different species and progress variable source term will be interpolated to calculate the other flow parameters. The turbulent flow field is modeled in OpenFOAM, [56] an open-source software, and Lib-ICE [57], a code based on OpenFOAM technology. OpenFOAM is a set of libraries and solvers developed for CFD simulations in a wide variety of applications. The OpenFOAM solvers integrate the spray models with an Eulerian-Lagrangian approach with sub-models for injection, atomization, breakup, and wall impingement. Lib-ICE focuses on internal combustion engine simulations developed by the Internal Combustion Engine (ICE) group of Politecnico di Milano. Both of them are programmed in C++ and then a class is implemented to retrieve the data stored in the tables and update the source term in the transport equation of the progress variable and the transport properties. For the turbulence modeling and closing the momentum equation in the CFD solver, the standard $k-\varepsilon$ turbulence model is adopted for predicting the turbulent kinetic energy (k) and the dissipation rate (ε) in the domain [58]. In this model, two additional transport equations are solved for k and ε. Subsequently, the Reynolds stress tensor is calculated from them.

Fig. 3 depicts a schematic representation of the proposed

Table 1
summary of the configuration used for counterflow diffusion flame.

Configuration name	Counterflow diffusion flame
Oxidizer composition (mass fraction)	0.15 O_2, 0.7515 N_2, 0.0623 CO_2, 0.0362 H_2O
Oxidizer Temperature	900 K
Pressure	60 bar
Chemical kinetic mechanism	54 species and 269 reactions) [60]

methodology and summarizes the procedure discussed in the previous sections.

For the numerical solution, the governing equations need to be discretized over the computational grid. For the time derivative, the Euler method which is a transient, bounded, and first-order implicit scheme was used. For the gradient terms, the Gauss linear scheme which is second order with Gaussian integration discretization with linear interpolation was utilized. The Gauss scheme is used for the discretization of Laplacian terms with an added correction to account for the areas in the mesh which are less orthogonal. For divergence terms, linear upwind was used; however, when the algorithm generates values outside the physical range, a limited scheme was adopted to avoid non-physical solutions.

3. Results and discussion

To assess the quality of the optimum PV definition, in the first step, the igniting one-dimensional CDF is recomputed by applying the FGM table. This will give a validation of the approach since it can be compared to the solution of fully detailed kinetics. In the second step, ECN Spray A will be simulated to analyze the effect of the PV definition approach on the ignition delay and the lift-off length predictions.

3.1. One-dimensional counterflow flame: a priori analysis

ECN Spray A operating condition of 15% O_2, 22.8 kg/m^3 is initialized in the flamelet and the CFD simulation which mimics a typical condition of IC engines before the start of combustion [47]. A counterflow unsteady igniting configuration is tested for the performance of the optimum FGM model. Conventional one-dimensional counterflow diffusion flame may also serve as a conical configuration for conventional diesel engines. The corresponding oxidizer composition is also chosen to mimic the oxidizer composition in the corresponding combustion engine. This transient problem needs an initial solution. For the initial solution, the system was solved first without considering combustion (i.e. the mixing solution) and its solution is used as the initial condition for the unsteady simulation. Table 1 summarizes the configuration and the mechanism used. The fuel temperature was set to 155 K to account for the heat loss due to the spray evaporation as discussed in [34]. The mechanism selected is reduced versions in order to keep the runtime and the memory requirement low for all the cases. The mechanisms have been validated extensively to model n-dodecane combustion in different research works for ignition delay and laminar flame speed predictions [59,60].

The solution of laminar diffusion flamelets builds the basis for the later CFD simulation discussed in the previous sections. The results of the proposed optimization approach are evaluated and compared with two commonly used definitions (PV1 and PV2) and a progress variable (PV3) which has been already optimized manually by a previous study [34] :

$$PV1 = Y_{CO_2} + Y_{CO} + Y_{H_2} + Y_{H_2O} \tag{13}$$

$$PV2 = Y_{CO_2} + Y_{CO} \tag{14}$$

$$PV3 = 1.2Y_{CO_2} + 0.9Y_{CO} + 2.7Y_{HO_2} + 1.5Y_{CH_2O} + 1.2Y_{H_2O} \tag{15}$$

Subsequently, the monotonicity is analyzed, and the main species profiles are evaluated in more detail. Since the oxidizer contains some amount of CO_2 and H_2O, the progress variable is not zero at the boundary side of the oxidizer, where there are almost no reactions. Therefore to make the FGM simulation more convenient, the progress variable was normalized to be zero at the oxidizer side.

The FGM table used here has 500 grid points in PV, and 300 grid points in Z. Fig. 4 shows the cost value of the best individual in each generation. The cost value is the negative value of the merit function defined in Eq. (10). The algorithm starts with an initial random solution shown by a blue triangle. As we can see, PV1 (purple triangle) and PV2 (green triangle) have lower cost values compared to the initial random solution, which means that they result in a smaller non-monotonicity region. This implies that a knowledge-based choice actually can have better results in terms of the monotonicity of the progress variable. The non-monotonicity region is indicated by the white areas in the contour plots. PV3 (crimson triangle), which is already optimized manually for an n-dodecane counterflow diffusion flame, leads to significant improvement in the monotonicity of the progress variable implying the importance of optimization of PV. The orange triangle shows the cost value of the best solution among all solutions after the first iteration of the algorithm. After the first iteration, the algorithm finds a progress variable definition with a very low-cost value. Note that the algorithm,

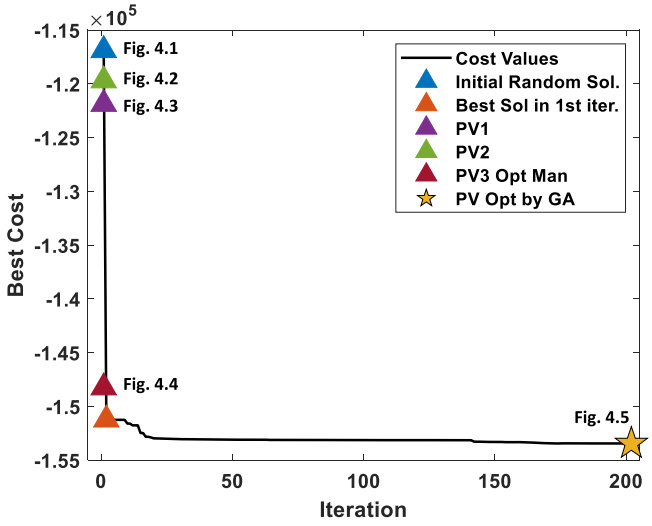

Fig. 4. Evolution of the best solution in each generation (iteration).

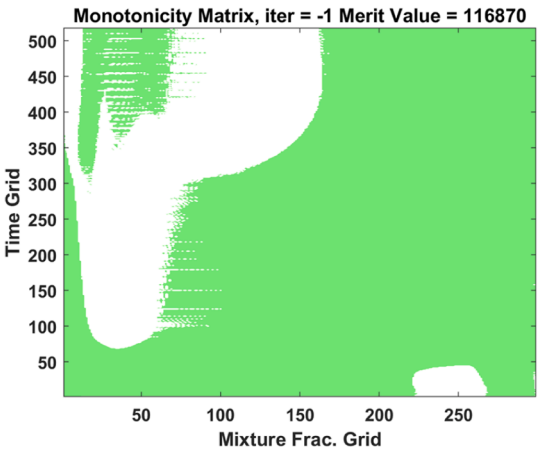

Fig. 4.1 non-monotonicity area of the initial random PV (blue triangle in Fig. 4)

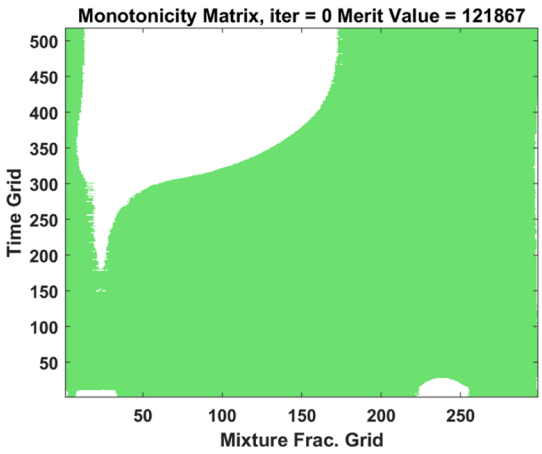

Fig. 4.2 non-monotonicity area of PV1 (green triangle in Fig. 4)

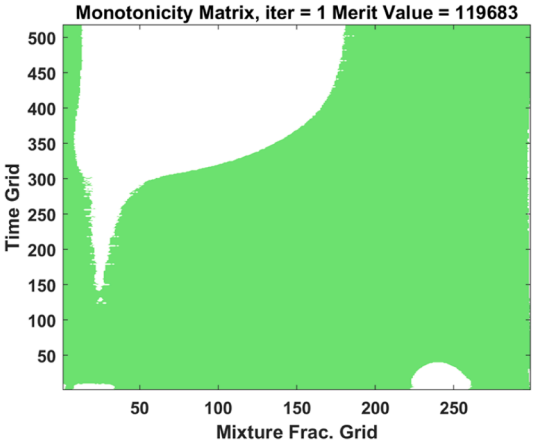

Fig. 4.3 non-monotonicity area of PV2 (purple triangle in Fig. 4)

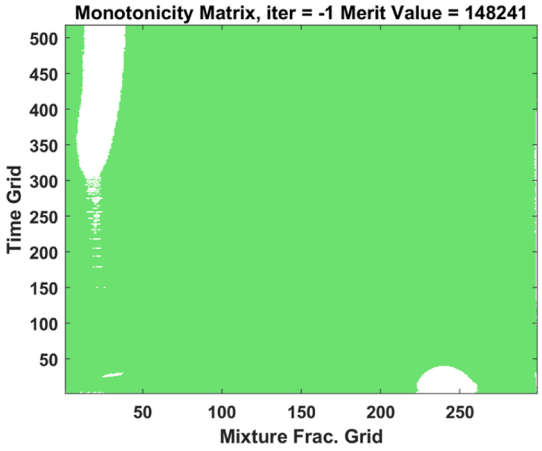

Fig. 4.4 non-monotonicity area of PV3 (red triangle in Fig. 4)

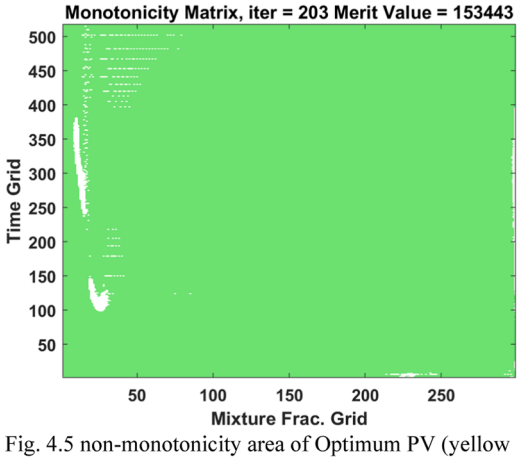

Fig. 4.5 non-monotonicity area of Optimum PV (yellow star in Fig. 4)

Fig. 4. (*continued*).

after the first 20 iterations, has already reached a cost value very close to the final optimum solution represented by the golden star in the figure. The optimum coefficients after 200 iterations have been shown in the table in Appendix B. and Nitrogen gas and Argon was set to zero. It is worth mentioning that the whole process for the 200 iterations took only around 6 min on a single processor.

The performance of the optimum PV definition found by the algorithm was evaluated at different temperature and pressure levels. Fig. 5-a shows the ignition delay prediction resulting from both the detailed kinetic approach and the FGM modeling with the optimum progress variable. The ignition delay was defined as the time when the OH concentration reaches 2 percent of the maximum value throughout the complete simulation. The FGM results almost match the detailed kinetic results except at lower temperatures where a small difference exists. As it has been reported in [60], the chemical kinetic mechanism does not result in accurate ignition delay prediction in lower temperatures.

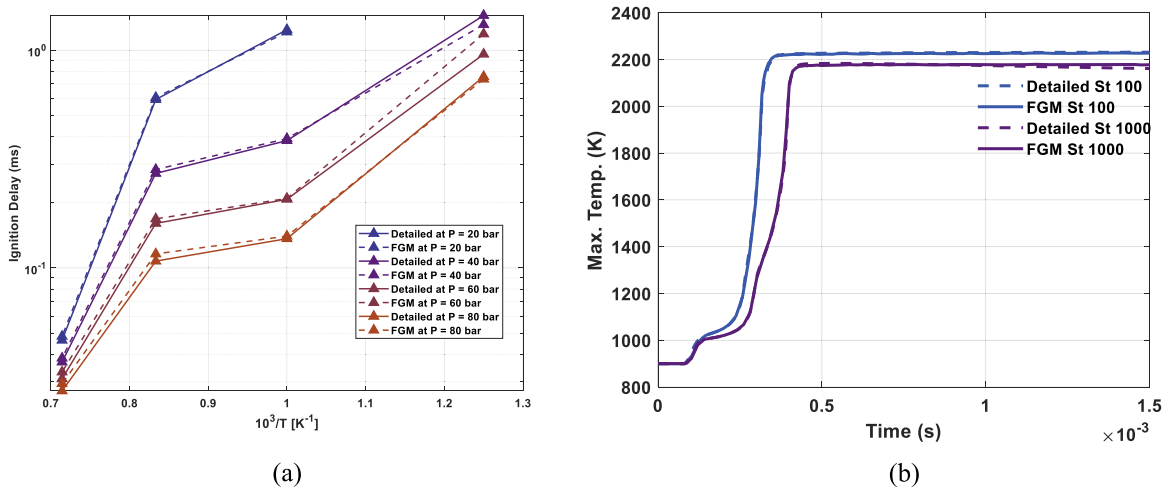

Fig. 5. (a) ignition delay counterflow diffusion flames at different pressures with a strain rate = 500 (1/s) and (b) maximum temperature profile for different strain rates for FGM and detailed kinetic approach.

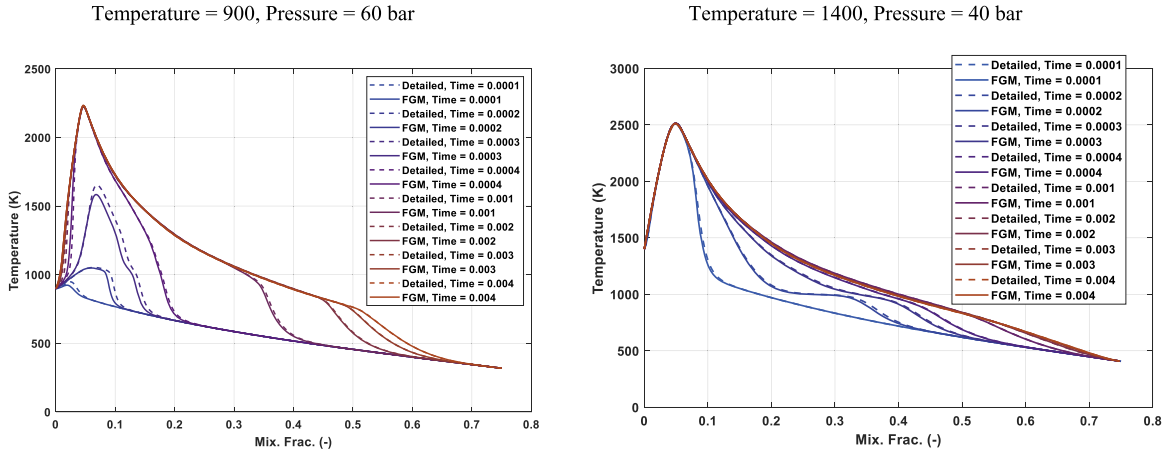

Fig. 6. Temperature as the function of Mixture fraction at Different Times [- - - Detailed, FGM].

Therefore both approaches, which are based on the mechanism, can have larger errors. Strain rate is another important parameter that affects mixing, emission formations, and other combustion characteristics like flame thickness and flame temperature. Therefore, the optimum definition should also capture the dependency on strain rate. Fig. 5-b shows the maximum temperature for two different strain rates. In both conditions, the FGM model has a negligible deviation from detailed kinetic results.

On an even more detailed level, Fig. 6 shows the evolution of the ignition of the complete flame by both the optimum FGM model and the detailed kinetic approach for two different operating conditions. At all shown times the FGM model is very close to the solutions provided by the detailed kinetics.

Fig. 7 shows the profiles connecting the maximum temperature values and the maximum of important species (including C_2H_2, CH_2O, CO_2, HO_2, CO, and OH) in different timesteps as a function of time. The accurate prediction of C_2H_2 is essential since it is usually used in soot formation predictions as a gas-phase soot precursor in most soot models [30]. CH_2O usually appears during the initial heat release associated with the early stage of fuel decomposition [16]. HO_2 is another key species because the ignition process starts with the formation of HO_2, and OH distribution in the domain is a metric to calculate important combustion characteristics such as ignition delay and flame lift-off length. Using PV1 and PV2 the ignition delay is overpredicted in almost all the cases because of the underprediction of the source term of the progress variable equation by these two definitions as we will see in the next section. There is a slight shift in the prediction of species profiles using PV1 and PV2 which is because of the ID difference. The optimum PV accurately captures the timing of both the first and the second stages of the ignition process. It can be seen that the maximum species profiles either shifted due to the ID prediction differences or have a completely different shape like C_2H_2 and CO when PV is not optimized. The maximum temperature result of PV3 in a different strain rate (500 s^{-1}), which is optimized empirically was also compared with the optimum PV in a separate Figure (Fig. 8). It was also found that manually optimized performs well in lower strain rate. However, when the strain rate is increased its accuracy decrease significantly. The optimum PV performs much better in both conditions compared to the other PVs especially when the strain rate is changed. The species mass fraction profiles of other PV definitions significantly differ from the detailed results especially in the higher strain rate, indicating the significance of the PV definition. However, the results of other PV definitions in higher strain rate was not represented here for the sake of brevity.

The progress variable source for the optimized PV and the three manually selected PV definitions are presented in Fig. 9 as a function of the progress variable and the mixture fraction. Since the oxidizer contains some amount of CO_2 and H_2O, the progress variable is not zero at the boundary side of the oxidizer, where there are almost no reactions. Therefore to make the FGM simulation more convenient, the progress variable was normalized to be zero at the oxidizer side. For reference,

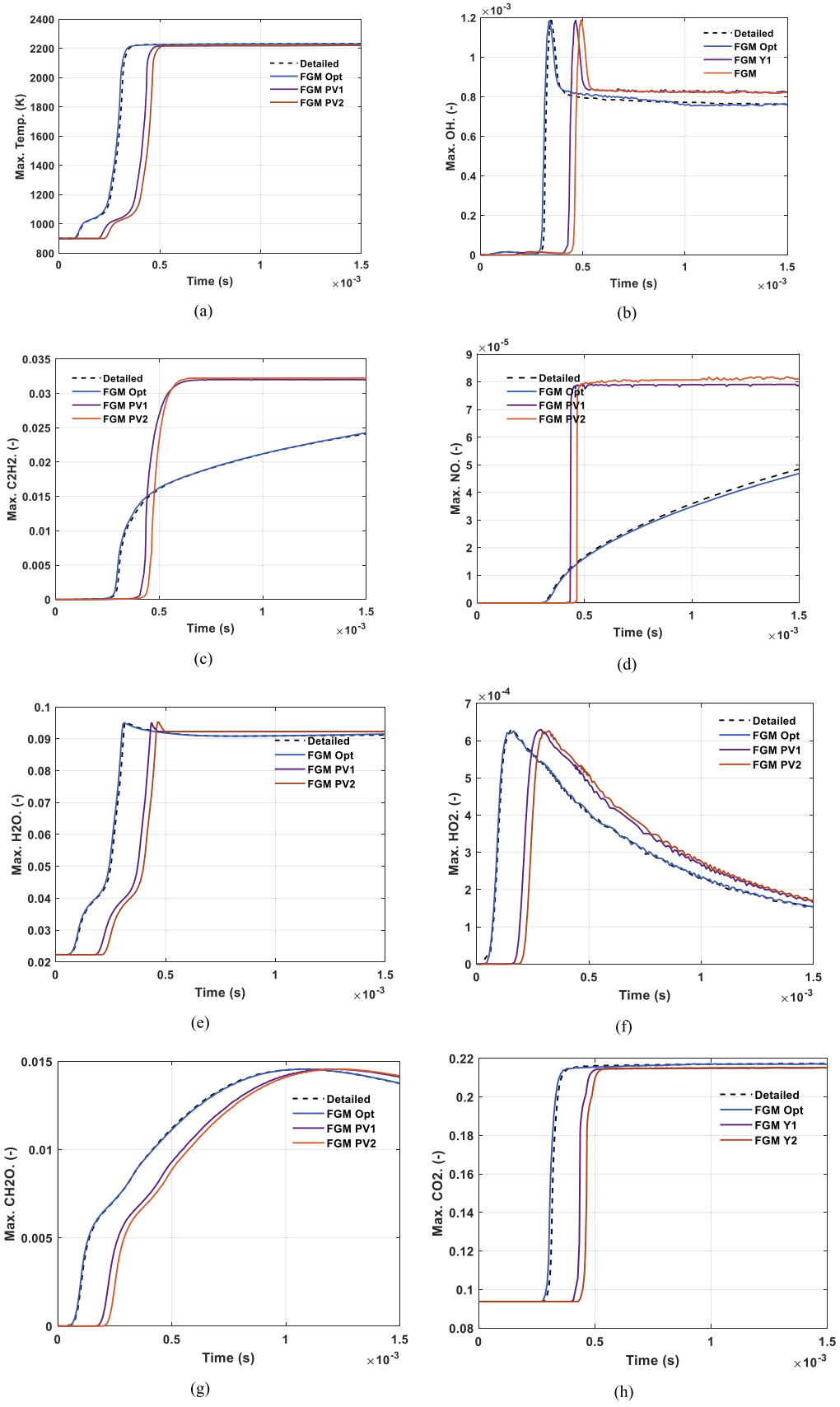

Fig. 7. Temperature and Important Species Prediction of Detailed and FGM Modeling with two conventional PV and the optimized PV. The strain rate of 100 (1/s).

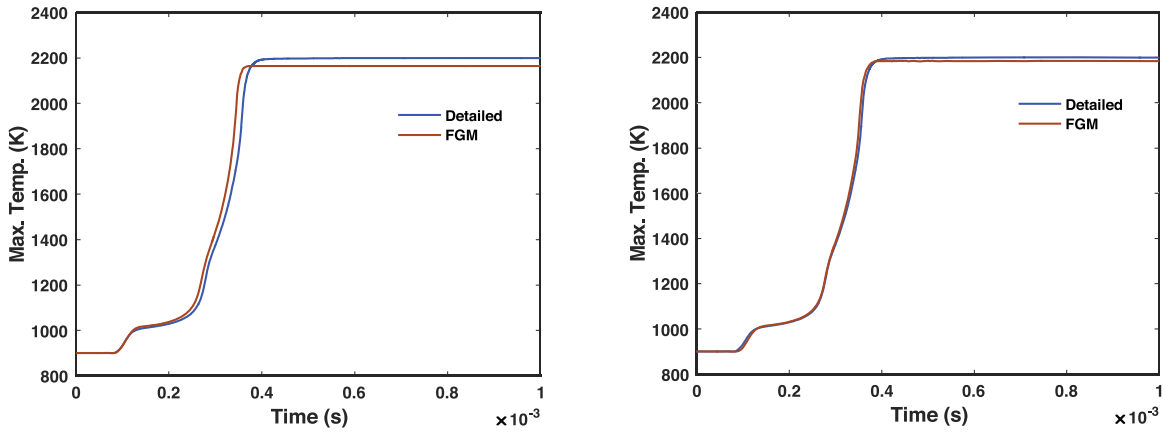

Fig. 8. Maximum Temperature Prediction of Detailed and FGM with manually optimized PV (left) and automatically optimized PV (right) using GA. The strain rate of 500 (1/s).

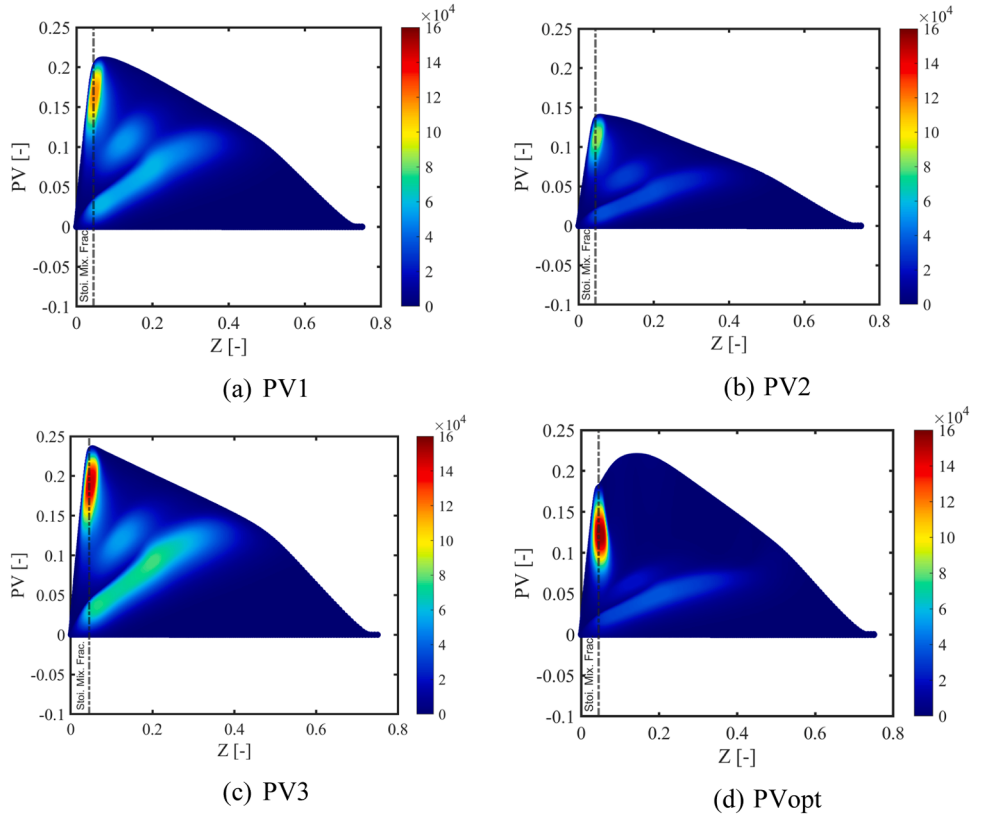

Fig. 9. PV source as function of Progress variable definition and mixture fraction (a) PV1 (b) PV2 (c) manually optimized PV3 (d) automatically Optimized PV with GA.

Table 2
The turbulence model coefficients used in the current study.

Coefficient	C_μ	C_1	C_2	σ_k	σ_ε
value	0.09	1.5	1.92	1.0	1.4

the stoichiometric mixture fraction value is also depicted by a dashed vertical line. The contour plot shows that the PV source is highly dependent on the PV definition, and with the two non-optimized PV (PV1 and PV2), the maximum value of the source term was much lower than the source term of the other two optimized definitions. This large difference can cause the ignition to happen much later, which is already shown in the previous section. The maximum PV source happens near

Table 3
The summary of the adopted sub-models in the CFD simulation.

Phenomenon	Model	Reference
Turbulence flow	Standard $k-\varepsilon$	[58]
Spray secondary break up	KH-RT	[66]
Evaporation model	Multi-component vaporization	[68]
Combustion model	FGM	[19]
Combustion chemical kinetic	Yao Mechanism (54 species and 269 reactions)	[60]

Table 4
The ECN spray A validation summary.

Ambient gas temperature (K)	800, 900 (Section 3.1), 1000
Ambient gas pressure (MPa)	~ 6.0
Ambient gas density (kg/m^3)	22.8
Ambient gas oxygen (by vol.)	15% O_2
Ambient gas velocity (m/s)	Near-quiescent, < 1 m/s
Common rail fuel injector	Bosch solenoid-activated
nozzle outlet diameter (mm)	0.09
Discharge coefficient (-)	0.86
Number of holes (-)	1
injection pressure (MPa)	150
Fuel Name	N-Dodecane
Fuel temperature at the nozzle (K)	363
Injection duration (ms)	6.0
Injected Mass (mg)	14

the stoichiometric value. It can also be noticed that with PV1 and PV3, there are some higher reactive areas in the rich region.

3.2. CFD modeling spray A

The effect of the optimum progress variable in the CFD model is also evaluated and the results were compared with the experimental data. Consistent and reliable experimental data are a prerequisite for validating simulation models. The ECN experiments span a wide range of fuels and configurations. Internal combustion engines usually operate at elevated temperatures and pressures. The construction of the combustion chamber is generally very complex and inaccessible to optical sensors and instruments. Moreover, the length and time scales of turbulent fluid dynamics and combustion necessitate spatial and temporal data with very high resolutions. All these factors make it extremely difficult to obtain accurate experimental data for turbulent flames at higher pressures. The ECN standardized experimental conditions would allow comparative study between different modeling frameworks and codes and establish best practices.

Thanks to the circumferential symmetry of the nozzle of the ECN Spray A (Although this is not entirely true, its effect on the spray evolution and flow is negligible [61]), a wedge geometry was created to improve the computational efficiency as also used in [62,63]. The mesh is refined near the nozzle region, where the gradient of the flow variables is high. The standard $k-\varepsilon$ turbulence model is utilized with the coefficients listed in Table 2. The coefficients were calibrated in the previous study [64]. The pressure and velocity equations are coupled by the PIMPLE algorithm implemented in OpenFOAM [65]. Furthermore, the Euler-Lagrangian approach is utilized for spray modeling. When the fuel injection takes place, the fuel droplets enter the combustion chamber and subsequently, these droplets undergo a breakup process. In this study, this process is modeled by the Kelvin-Helmholtz and Rayleigh-Taylor (KH-RT) instabilities. This model consists of two stages. In the first step, the KH instability model is used to calculate the size of new droplets (child droplets). Then, after a certain length from the injector (break-up length), the RT model is activated and calculates the size of the newer generated droplets from parent droplets [66]. Heat transfer between the droplets and the surrounding gas is simulated according to the Ranz-Marshall model [67]. For the evaporation and the drag force applied to the droplets, the standard evaporation and drag models defined in the OpenFOAM are used. The grid dependency study and the calibration of the spray submodels have been done in the previous study [64]. Table 3 summarizes the submodels used in the current study.

In order to validate the CFD model, three different operating conditions similar to those observed in conventional diesel engines are selected from the ECN experimental results. Table 4 summarizes these conditions. First, these conditions are set to create the flamelets. Then the data are retrieved in the CFD model to calculate the species concentration and the progress variable source term as already described in the previous sections.

One of the essential parameters for Spray A is the ignition delay (ID), which is the time between fuel injection and the start of combustion. Since the injection timing and the start of combustion can be specified according to several criteria, different definitions for this parameter

Table 5
Error analysis of the CFD prediction.

FLOL (mm)	Rel. Error (%)	ID (ms)	Rel. Error (%)	Oxidizer Temperature (K)	
26.2	–	0.85	–	800	Exp
27.0	3	1.16	36	800	Sim (PV opt)
23.4	11	1.28	51	800	Sim (PV3)
16.7	–	0.41	–	900	Exp
16.0	4	0.4	2.4	900	Sim (PV opt)
13.9	17	0.42	2.4	900	Sim (PV3)
12.2	–	0.24	–	1000	Exp
12.0	1.6	0.22	8	1000	Sim (PV opt)
11.0	9.8	0.23	4	1000	Sim (PV3)

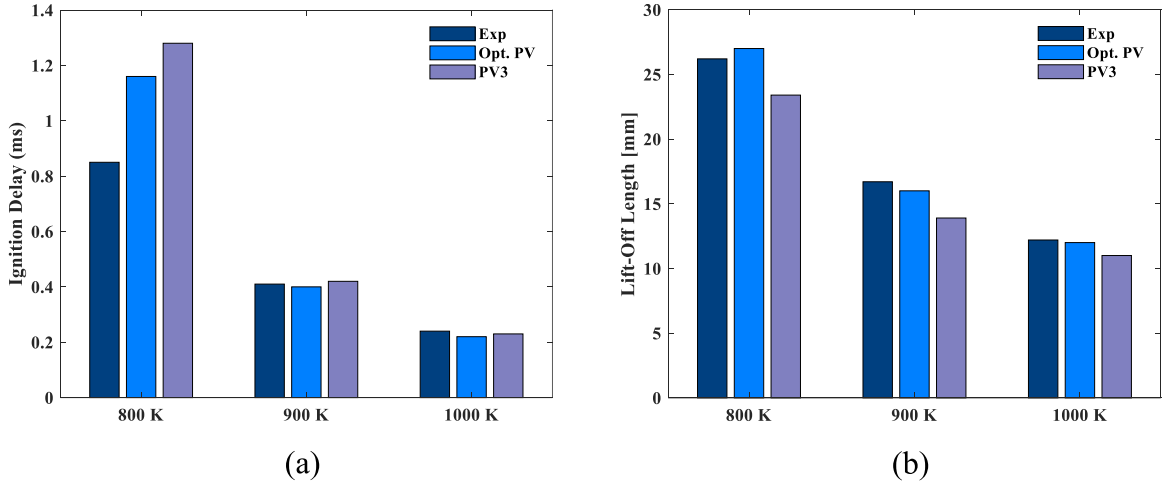

Fig. 10. (a) Ignition Delay (ID) (b) Flame Lift-Off Length (FLOL) comparison of the manually optimized PV and the automatically optimized PV in three different operating temperatures.

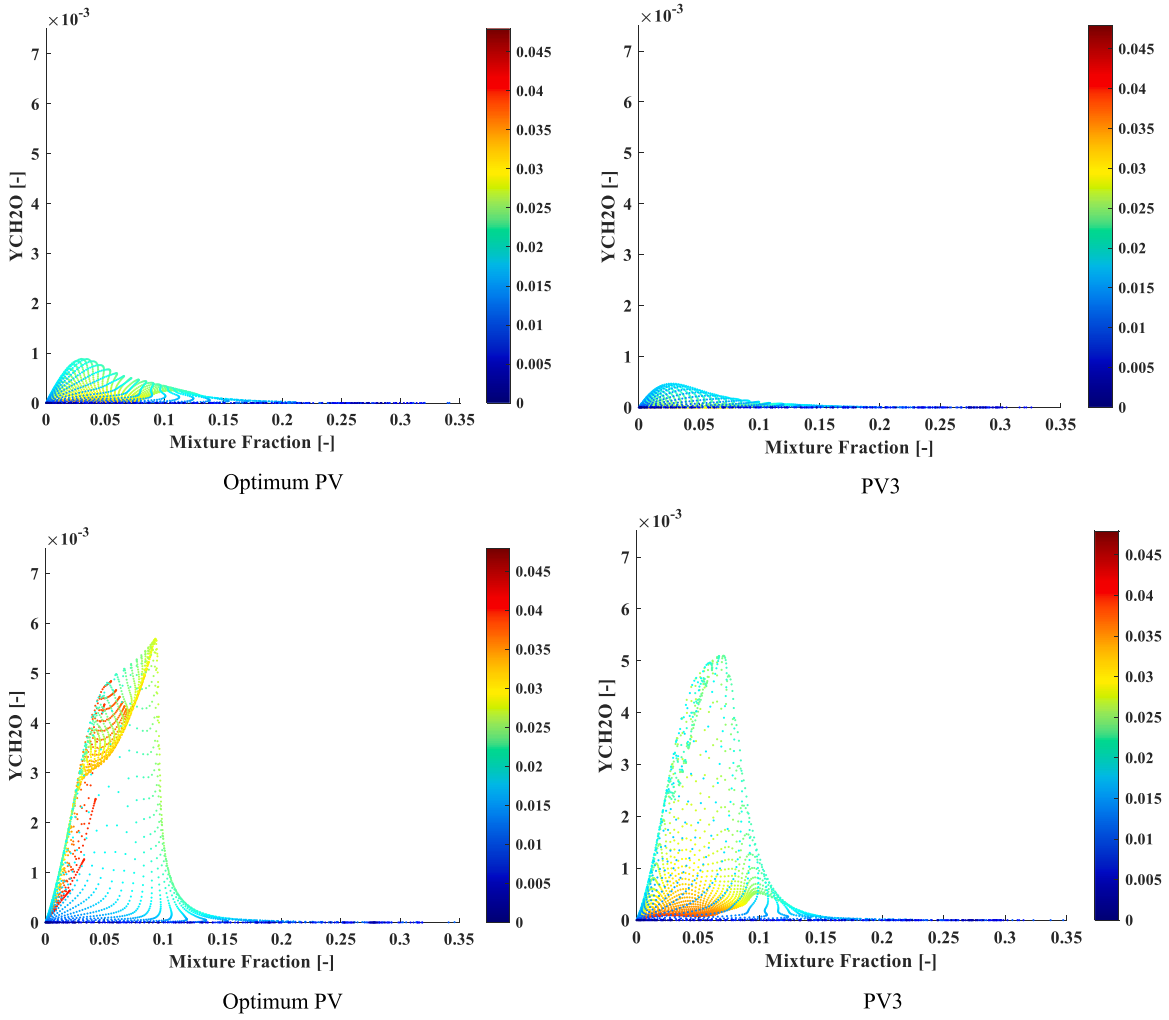

Fig. 11. The Formaldehyde distribution against the mixture fraction colored by the axial distance from the nozzle at the oxidizer temperature of 800 K. Top row: at 0.85 ms bottom row: at 1.05 ms.

have been presented in the literature. In the current study, ID is defined when the maximum OH concentration in the domain reaches 2% of its maximum value throughout the flame stabilization period. Besides ID, Flame Lift-Off Length (FLOL) is another crucial parameter that defines the distance from the nozzle to the most upstream of the flame. FLOL indirectly affects the emission formation in diffusion flame combustion. Again there are several ways to define the most upstream of the flame. In this work, FLOL is defined as the minimum axial distance from the nozzle where OH concentration reaches 14% of its maximum value throughout the domain at the flame stabilization point. Both ID and FLOL follow the recommended definitions by the Engine Combustion Network [47].

Fig. 10 represents the results of the ID and FLOL calculated by the CFD model with both the Optimum progress variable and PV3, which is manually optimized. The model with PV1 and PV2 does not ignite, which shows that the wrong choice of PV leads to the inability of the model to simulate combustion. This is mainly because of the under-prediction of PV source terms when PV1 and PV2 are used, as already shown in Fig. 9. As can be seen, the FGM combustion model with the progress variable optimization method can predict the experimental results with reasonable accuracy. The relative error is reported in Table 5. ID prediction at the lower temperature deviates from the experimental data. This can be attributed to the chemical mechanism itself, which fails to produce accurate results in low temperatures, as we discussed earlier, and not the current approach. In CFD simulations, in addition to combustion, many other physical, transport, and chemical phenomena also involve. In one-dimensional and zero-dimensional simulations, many of these phenomena do not exist. In the part of the one-dimensional simulation of this research as well as the research done by Yao [60], it was shown that the combustion modeling with the used mechanism has a larger error at lower temperatures. Therefore, it is assumed that one of the important reasons for this difference is the chemical mechanism. The value predicted by optimum PV found automatically by the algorithm is closer to the experimental data, and PV3 results in a more significant deviation in the low oxidizer temperature of 800 K. IDT at the higher temperatures is almost the same by the two PV definitions. However, the lift-off length results imply that the optimum PV found by the current approach can lead to final better predictions in all the oxidizer temperature levels. This is mainly because of the better prediction in species mass fraction, especially RO_2 and OH, and lower non-monotonicity by the PV definition found by the current approach, as already shown in the previous sections. RO_2 is an indicator of the start and the end time of the cool flame period.

Fig. 11 compares the formaldehyde (CH_2O) distribution of the FGM results of the optimum PV with PV3 in two different time instances at the oxidizer temperature of 800 K. This oxidizer temperature was chosen for visualization since the IDT and FLOL values of the two progress variables have more difference so the effect of the optimization can be understood better. Formaldehyde is an essential intermediate species that defines the first combustion stage at relatively low temperatures. The dots in the

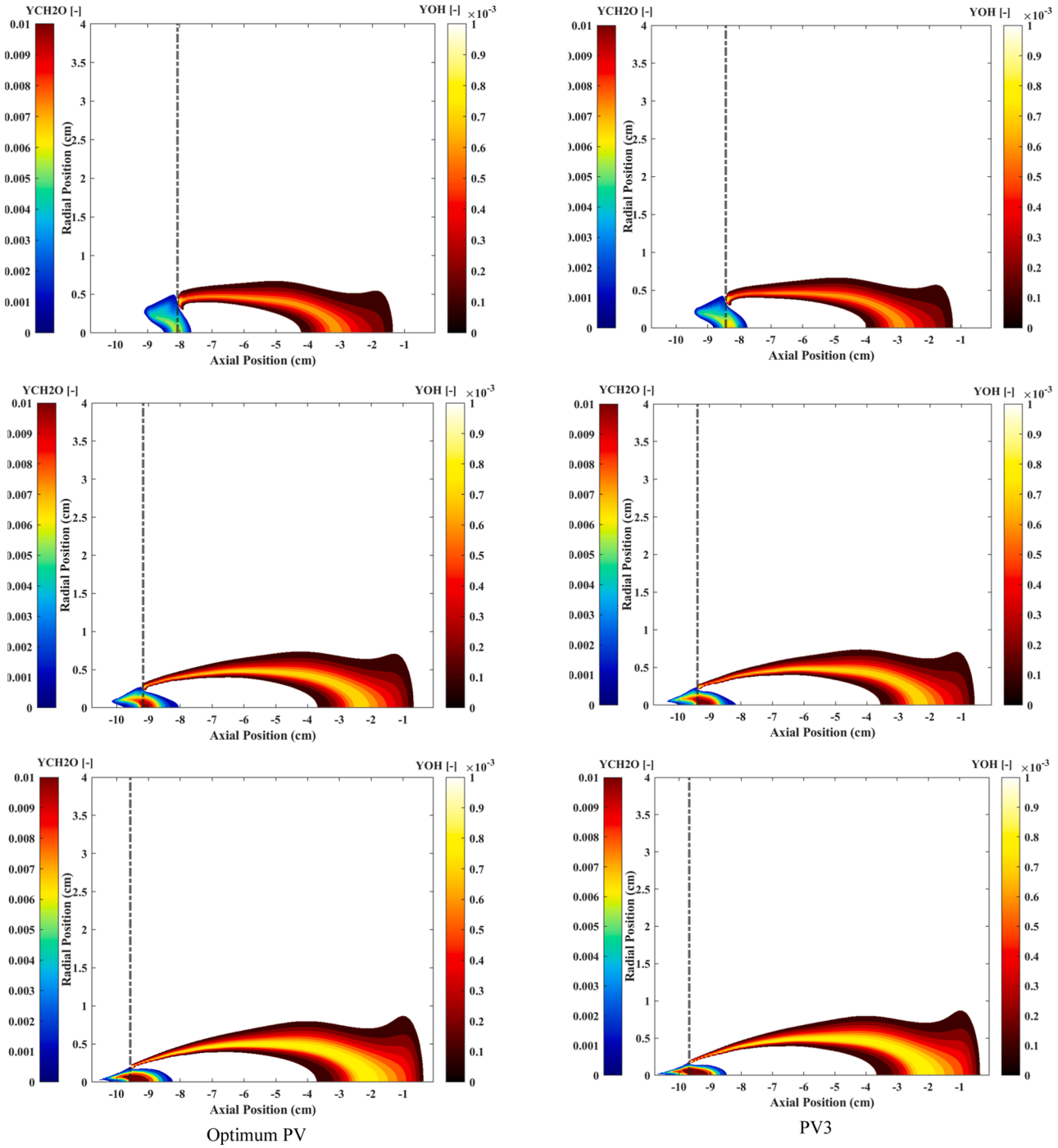

Fig. 12. The contours of formaldehyde (CH_2O) and hydroxyl (OH) mass fraction in three different oxidizer temperatures top row: at 800 K, middle row: 900 K, bottom row: 1000 K. The dash-dotted vertical lines indicate the location of FLOL.

Table A.1
GA tuned parameters.

Number of Population	10
Crossover Percentage	90
Mutation Percentage	15
Mutation Rate	0.01
Selection Pressure	3

figure have been colored by axial distance from the nozzle. As can be noticed, the optimization of the progress variable has a significant effect on the distribution of this species. Before the ignition time, the value predicted by the optimum PV is higher than the value predicted by PV3, which also justifies the earlier ignition delay timing with the optimum PV. In addition, it can be seen that CH_2O has higher values at the richer mixture fractions and also the longer distances from the nozzle with the optimum PV compared to PV3, and the use of PV3 results in the formation of less CH_2O at the spray tip before the ignition timing.

Fig. 12 represents the FGM model results using the optimum PV and PV3 in three different oxidizer temperatures at the end of the injection timing. Two different contours colored by the mass fractions of formaldehyde and OH are included in the figure. The contour demonstration of OH mass fraction helps to understand the location of the high reactive areas. The vertical dash-dotted lines show the location of FLOL. The

Table B.1
Optimum Coefficients found by GA.

N2	0	PC4H9	1.4775
AR	0	C5H9	1.6412
H	1.7072	C5H10	1.297
O	1.7969	PXC5H11	1.5138
OH	1.1866	C6H12	1.639
HO2	1.3669	PXC6H13	1.3918
H2	1.6176	C7H14	1.6943
H2O	2.0172	PXC7H15	1.585
H2O2	1.3851	C8H16	1.1535
O2	0.28921	PXC8H17	1.454
CH2	1.5875	C9H18	1.7457
CH2*	1.6628	PXC9H19	1.1763
CH3	1.6141	C10H20	1.0346
CH4	2.0425	PXC10H21	1.423
HCO	1.4769	NC12H26	1.2997
CH2O	0.96212	PXC12H25	1.4382
CH3O	1.7944	SXC12H25	1.5363
CO	0.24922	S3XC12H25	1.3244
CO2	1.2635	C12H24	1.3408
C2H2	2.7322	C12H25O2	1.5928
C2H3	1.5179	C12OOH	1.1834
C2H4	1.704	O2C12H24OOH	1.4982
C2H5	1.503	OC12H23OOH	1.4721
C2H6	1.2819	NO	2.7696
CH2CHO	1.8844	N2O	1.5436
AC3H5	1.6371	NO2	1.424
C3H6	1.1985	N	1.5394
NC3H7	1.6555		
C2H3CHO	1.4171		
C4H7	1.947		
C4H81	1.2055		

right column shows the PV3 results. The value of the CH_2O mass fraction is higher with PV3, and the area of high CH_2O is more stretched in the axial direction. The area of high OH concentration is also more stretched in the axial direction. This is more obvious in the lower oxidizer temperatures. Moreover, formaldehyde forms more upstream of the FLOL location. The reasons for the differences between the two cases are the differences in local temperatures and the value of the source term of PV prediction by PV3 and the optimum PV. With respect to the effect of the oxidizer temperature, the structure of the area of the two species and their maximum values are highly affected by temperature. At higher oxidizer temperatures, CH_2O consumes further downstream of FLOL and closer to the spray axis. OH forms closer to the nozzle location and the spray axis at higher temperatures.

4. Conclusion

The FGM approach has been used as one of the flamelet approaches to define a global formula for the progress variable (PV) with a genetic algorithm optimization. The results have been compared with two conventional Progress Variable definitions and one already manually optimized definition. It has been found with the use of an optimum progress variable in the model, the tremendous and time-consuming task of finding an appropriate progress variable by the user is eliminated. In the proposed method, the user does not need to have deep knowledge about the combustion system being simulated and can gain higher accuracy results in much less time than when other manually selected PV definitions are used. The accuracy of this method has been tested in three different operating conditions. The ignition delay time, the flame lift-off length, and the species concentration results have been compared with the detailed kinetic model and the ECN Spray A experimental data in both a 1D counter flow and a CFD simulation of non-premixed diffusion flame. The results show that the proposed approach is able to reproduce the results of the detailed kinetic combustion model and the experimental data with very high accuracy in all the operating conditions, and the non-monotonicity area is reduced significantly compared to all the other three PV definitions. The two conventional PVs failed to capture ignition in the CFD model and led to very late ignition in the 1D model due to underprediction in the PV source term. Comparison with the manually optimized definition also showed that the optimum found by the current approach could result in a much better prediction of combustion characteristics and has a significant effect on the species distribution in the domain. Since the algorithm needs to be executed before the chemistry tabulation in the pre-processing step, it does not increase the runtime of the FGM simulation. The algorithm itself only needs a few minutes to be finished on a standard desktop. The current approach is applicable to other combustion configurations with multiple fuels and reactant streams.

Declaration of Competing Interest

The authors declare that they have no known competing financial interests or personal relationships that could have appeared to influence the work reported in this paper.

Data availability

The optmization code is available in https://gitlab.tue.nl/.

Acknowledgments

This work was funded by the Netherlands Organisation for Scientific Research (NWO, project number 14927).

Appendix A

Table A.1

Appendix B

Table B.1

References

[1] Lucchini T, Della Torre A, D'Errico G, Onorati A. Modeling advanced combustion modes in compression ignition engines with tabulated kinetics. Appl Energy 2019; 247:537–48.
[2] Göktolga MU, de Goey P, van Oijen J. Modeling Temperature Variations in MILD Combustion Using MuSt-FGM. Front Mech Eng 2020;6:6.
[3] Kakaee A-H, Rahnama P, Paykani A. CFD study of reactivity controlled compression ignition (RCCI) combustion in a heavy-duty diesel engine. Period Polytech Transp Eng 2015;43:177–83.
[4] Efimov D.V. Taking flamelet generated manifolds to a higher dimension: reduced combustion modeling with multiple reactive time-scales. PhD Thesis. Technische Universiteit Eindhoven 2019.
[5] Cai L, vom Lehn F, Pitsch H. Higher alcohol and ether biofuels for compression-ignition engine application: a review with emphasis on combustion kinetics. Energy Fuels 2021;35:1890–917.
[6] De Bellis V, Malfi E, Lanotte A, Fasulo G, Bozza F, Cafari A, et al. Development of a phenomenological model for the description of RCCI combustion in a dual-fuel marine internal combustion engine. Appl Energy 2022;325:119919.
[7] Schluckner C, Gaber C, Landfahrer M, Demuth M, Hochenauer C. Fast and accurate CFD-model for NOx emission prediction during oxy-fuel combustion of natural gas using detailed chemical kinetics. Fuel 2020;264:116841.
[8] Luecke J, Rahimi MJ, Zigler BT, Grout RW. Experimental and numerical investigation of the Advanced Fuel Ignition Delay Analyzer (AFIDA) constant-volume combustion chamber as a research platform for fuel chemical kinetic mechanism validation. Fuel. 2020;265:116929.
[9] Ichikawa Y, Niki Y, Takasaki K, Kobayashi H, Miyanagi A. NH3 combustion using three-layer stratified fuel injection for a large two-stroke marine engine: experimental verification of the concept. Appl Energy Combust Sci 2022;10: 100071.
[10] Karimkashi S, Kaario O, Vuorinen V. Effects of hydrogen enrichment and turbulence intensity on the combustion mode in locally stratified dual-fuel mixtures of n-dodecane/methane. Appl Energy Combust Sci 2022;10:100072.
[11] Najt PM, Foster DE. Compression-ignited homogeneous charge combustion. SAE Transactions 1983;92:964–79.
[12] Noehre, C., Andersson, M., Johansson, B., and Hultqvist, A., "Characterization of Partially Premixed Combustion" SAE Technical Paper 2006-01-3412, 2006, 10 .4271/2006-01-3412.

[13] Kokjohn SL, Hanson RM, Splitter DA, Reitz RD. Fuel reactivity controlled compression ignition (RCCI): a pathway to controlled high-efficiency clean combustion. Int J Engine Res 2011;12:209–26.
[14] Farhan SM, Wang P. Post-injection strategies for performance improvement and emissions reduction in DI diesel engines—a review. Fuel Process Technol 2022; 228:107145.
[15] Rahnama P, Paykani A, Reitz RD. A numerical study of the effects of using hydrogen, reformer gas and nitrogen on combustion, emissions and load limits of a heavy duty natural gas/diesel RCCI engine. Appl Energy. 2017;193:182–98.
[16] Rahnama P, Paykani A, Bordbar V, Reitz RD. A numerical study of the effects of reformer gas composition on the combustion and emission characteristics of a natural gas/diesel RCCI engine enriched with reformer gas. Fuel 2017;209:742–53.
[17] Paykani A, Kakaee AH, Rahnama P, Reitz RD. Progress and recent trends in reactivity-controlled compression ignition engines. Int J Engine Res 2015;17: 481–524.
[18] Maas U, Pope SB. Simplifying chemical kinetics: intrinsic low-dimensional manifolds in composition space. Combust Flame 1992;88:239–64.
[19] Van Oijen JA, De Goey LPH. Modelling of premixed counterflow flames using the flamelet-generated manifold method. Combust Theory Model 2002;6:463–78.
[20] van Oijen JA. Flamelet-generated manifolds: development and application to premixed laminar flames. Eindhoven University Press; 2002.
[21] Pitsch H, Barths H, Peters N. Three-dimensional modeling of NO x and soot formation in DI-diesel engines using detailed chemistry based on the interactive flamelet approach. SAE Trans 1996:p. 2010–24.
[22] D'Errico G, Lucchini T, Contino F, Jangi M, Bai XS. Comparison of well-mixed and multiple representative interactive flamelet approaches for diesel spray combustion modelling. Combust Theory Model 2014;18:65–88.
[23] Oijen JAV, Goey LPHD. Modelling of premixed laminar flames using flamelet-generated manifolds. Combust Sci Technol 2000;161:113–37.
[24] Wehrfritz A, Kaario O, Vuorinen V, Somers B. Large eddy simulation of n-dodecane spray flames using flamelet generated manifolds. Combust Flame 2016;167: 113–31.
[25] Ihme M, Chung WT, Mishra AA. Combustion machine learning: principles, progress and prospects. Prog Energy Combust Sci 2022;91:101010.
[26] Zadsirjan S, Tabejamaat S, Abtahizadeh E, van Oijen J. Large eddy simulation of turbulent diffusion jet flames based on novel modifications of flamelet generated manifolds. Combust Flame 2020;216:398–411.
[27] Gicquel O, Darabiha N, Thévenin D. Liminar premixed hydrogen/air counterflow flame simulations using flame prolongation of ILDM with differential diffusion. Proc Combust Inst 2000;28:1901–8.
[28] Pierce CD, Moin P. Progress-variable approach for large-eddy simulation of non-premixed turbulent combustion. J Fluid Mech 2004;504:73–97.
[29] Peters N. Turbulent combustion. Cambridge university press; 2000.
[30] Kalbhor A, van Oijen J. An assessment of the sectional soot model and FGM tabulated chemistry coupling in laminar flame simulations. Combust Flame 2021; 229:111381.
[31] Wan K, Vervisch L, Gao Z, Domingo P, Jiang C, Wang Z, et al. Reduced chemical reaction mechanisms for simulating sodium emissions by solid-fuel combustion. Appl Energy Combust Sci 2020;1-4:100009.
[32] Lucchini T, Pontoni D, D'Errico G, Somers B. Modeling diesel combustion with tabulated kinetics and different flame structure assumptions based on flamelet approach. Int J Engine Res 2019;21:89–100.
[33] Franzelli B, Vié A, Ihme M. On the generalisation of the mixture fraction to a monotonic mixing-describing variable for the flamelet formulation of spray flames. Combust Theory Model 2015;19:773–806.
[34] Akkurt B. Modelling multi-pulse diesel injection with flamelet generated manifolds. Eindhoven: Technische Universiteit; 2019.
[35] Bao H, Akargun HY, Roekaerts D, Somers B. The inclusion of scalar dissipation rate in modeling of an n-dodecane spray flame using flamelet generated manifold. Combust Flame 2023;249:112610.
[36] Verhoeven LM, Ramaekers WJS, Van Oijen JA, De Goey LPH. Modeling non-premixed laminar co-flow flames using flamelet-generated manifolds. Combust Flame 2012;159:230–41.
[37] Hoerlle CA, Zimmer L, Pereira FM. Numerical study of CO2 effects on laminar non-premixed biogas flames employing a global kinetic mechanism and the flamelet-generated manifold technique. Fuel 2017;203:671–85.
[38] Ihme M, Shunn L, Zhang J. Regularization of reaction progress variable for application to flamelet-based combustion models. J Comput Phys 2012;231: 7715–21.
[39] Fureby C, Bai X. Non-premixed and Partially Premixed Combustion Modeling. In: Swaminathan N, Bai X, Haugen N, Fureby C, Brethouwer G, editors. *Advanced Turbulent Combustion Physics and Applications*. Cambridge: Cambridge University Press; 2022. p. 162–99.
[40] Gupta H, Teerling OJ, van Oijen JA. Effect of progress variable definition on the mass burning rate of premixed laminar flames predicted by the flamelet generated manifold method. Combust Theory Model 2021:1–15.
[41] Meller D, Lipkowicz T, Rieth M, Stein OT, Kronenburg A, Hasse C, et al. Numerical analysis of a turbulent pulverized coal flame using a flamelet/progress variable approach and modeling experimental artifacts. Energy Fuels 2021;35:7133–43.
[42] Niu YS, Vervisch L, Tao PD. An optimization-based approach to detailed chemistry tabulation: automated progress variable definition. Combust Flame 2013;160: 776–85.
[43] Hadadpour A, Xu S, Pang KM, Bai X-S, Jangi M. Effects of pre-injection on ignition, combustion and emissions of spray under engine-like conditions. Combust Flame 2022;241:112082.
[44] Prüfert U, Hartl S, Hunger F, Messig D, Eiermann M, Hasse C. A constrained control approach for the automated choice of an optimal progress variable for chemistry tabulation. Flow Turbul Combust 2015;94:593–617.
[45] Vasavan A, de Goey P, van Oijen J. A novel method to automate FGM progress variable with application to igniting combustion systems. Combust Theory Model 2020;24:221–44.
[46] Chitgarha F, Ommi F, Farshchi M. Assessment of optimal reaction progress variable characteristics for partially premixed flames. Combust Theory Model 2022;26: 797–830.
[47] L.M. Pickett, G. Bruneaux, R. Payri, Engine Combustion Network, (https://ecn.sandia.gov/). Accessed 2022.
[48] de Goey LPH, ten Thije, Boonkkamp JHM. A flamelet description of premixed laminar flames and the relation with flame stretch. Combust Flame 1999;119: 253–71.
[49] Kee RJ, Miller JA, Evans GH, Dixon-Lewis G. A computational model of the structure and extinction of strained, opposed flow, premixed methane-air flames. Symposium (International) on Combustion. 1 ed. Elsevier; 1989. p. 1479–94.
[50] Stahl G, Warnatz J. Numerical investigation of time-dependent properties and extinction of strained methane and propane-air flamelets. Combust Flame 1991;85: 285–99.
[51] Somers B. The simulation of flat flames with detailed and reduced chemical models. Technical University of Eindhoven; 1994. Ph.D. Thesis.
[52] Kakaee A-H, Rahnama P, Paykani A, Mashadi B. Combining artificial neural network and multi-objective optimization to reduce a heavy-duty diesel engine emissions and fuel consumption. J Cent South Univ 2015;22:4235–45.
[53] Wirsansky E. Hands-on genetic algorithms with python: applying genetic algorithms to solve real-world deep learning and artificial intelligence problems. Packt Publishing Ltd; 2020.
[54] Buontempo F. Genetic algorithms and machine learning for programmers: create ai models and evolve solutions. Pragmatic Bookshelf; 2019.
[55] Rahnama P, Arab M, Reitz RD. A time-saving methodology for optimizing a compression ignition engine to reduce fuel consumption through machine learning. SAE Int J Engines 2020;13:267–88.
[56] Jasak H, Jemcov A, Tukovic Z. OpenFOAM: a C++ library for complex physics simulations. Int Workshop Coupled Methods Numer Dyn 2007;1000:1–20.
[57] Piscaglia F, Montorfano A, Montenegro G, Onorati A, Jasak H, Rusche H. Lib-ICE: a C++ object oriented library for ice simulation-acoustics and aftertreatment. Goteborg: Fifth OpenFOAM Workshop; 2011.
[58] Versteeg H.K., Malalasekera W. Introduction to Computational Fluid Dynamics, An: The Finite Volume Method, 2nd edition, Published by Pearson, February 5th 2007.
[59] Konnov AA. Yet another kinetic mechanism for hydrogen combustion. Combust Flame 2019;203:14–22.
[60] Yao T, Pei Y, Zhong B-J, Som S, Lu T, Luo KH. A compact skeletal mechanism for n-dodecane with optimized semi-global low-temperature chemistry for diesel engine simulations. Fuel 2017;191:339–49.
[61] Desantes, J., Payri, R., Gimeno, J., and Marti-Aldaravi, P., "Simulation of the First Millimeters of the Diesel Spray by an Eulerian Spray Atomization Model Applied on ECN Spray A Injector," SAE Technical Paper 2014-01-1418, 2014, 10.4271/2014-01-1418.
[62] Maghbouli A. Development of an advanced multi-dimensional CFD framework for modeling low temperature combustion in direct injection compression ignition engines. 2017. PhD Thesis, Politecnico di Milano, Department of Energy, http://hdl.handle.net/10589/132754.
[63] Torelli R, D'Errico G, Lucchini T, Ikonomou V, McDavid RM. A spherical volume interaction DDM approach for diesel spray modeling. Atomization and Sprays 2015;25:335–74.
[64] Maghbouli A, Akkurt B, Lucchini T, D'Errico G, Deen NG, Somers B. Modelling compression ignition engines by incorporation of the flamelet generated manifolds combustion closure. Combust Theory Model 2019;23:414–38.
[65] Holzmann T. Mathematics, numerics, derivations and openfoam®. Loeben, Germany: Holzmann CFD; 2016.
[66] Beale JC, Reitz RD. Modeling spray atomization with the Kelvin-Helmholtz/Rayleigh-Taylor hybrid model. At Sprays 1999;9.
[67] Marshall WR, Ranz WE. Internal combustion engine modeling. New York: Hemisphere Publishing; 1952.
[68] Greenshields CJ. OpenFOAM user guide version 10. The OpenFOAM Foundation; 2022.
[69] Li K., Rahnama P., Novella R., Somers B. Combining Flamelet Generated Manifold and Machine Learning Models in Simulation of a Non-Premixed Diffusion Flame. Energy and AI 2023. Under revision.